JACS
JOURNAL OF THE AMERICAN CHEMICAL SOCIETY
Article
pubs.acs.org/JACS

Stimuli Responsive Hybrid Magnets: Tuning the Photoinduced Spin-Crossover in Fe(III) Complexes Inserted into Layered Magnets

Miguel Clemente-León,*[,†] Eugenio Coronado,*[,†] Maurici López-Jordà,[†] João C. Waerenborgh,[‡] Cédric Desplanches,[§] Hongfeng Wang,[§] Jean-François Létard,[§] Andreas Hauser,[∥] and Antoine Tissot[∥]

[†]Instituto de Ciencia Molecular (ICMol), Universidad de Valencia, Catedrático José Beltrán 2, 46980 Paterna, Spain
[‡]IST/ITN, Instituto Superior Técnico, Universidade Técnica de Lisboa, CFMC-UL, 2686-953 Sacavém, Portugal
[§]Université de Bordeaux, ICMCB, 87 avenue du Dr. A. Schweitzer, Pessac, F-33608, France
[∥]Département de Chimie Physique, Université de Genève, 30 Quai Ernest-Ansermet, CH-1211 Genève 4, Switzerland

Supporting Information

ABSTRACT: The insertion of a $[Fe(sal_2\text{-trien})]^+$ complex cation into a 2D oxalate network in the presence of different solvents results in a family of hybrid magnets with coexistence of magnetic ordering and photoinduced spin-crossover (LIESST effect) in compounds $[Fe^{III}(sal_2\text{-trien})][Mn^{II}Cr^{III}(ox)_3]\cdot CHCl_3$ (**1·CHCl$_3$**), $[Fe^{III}(sal_2\text{-trien})][Mn^{II}Cr^{III}(ox)_3]\cdot CHBr_3$ (**1·CHBr$_3$**), and $[Fe^{III}(sal_2\text{-trien})][Mn^{II}Cr^{III}(ox)_3]\cdot CH_2Br_2$ (**1·CH$_2$Br$_2$**). The three compounds crystallize in a 2D honeycomb anionic layer formed by Mn^{II} and Cr^{III} ions linked through oxalate ligands and a layer of $[Fe(sal_2\text{-trien})]^+$ complexes and solvent molecules ($CHCl_3$, $CHBr_3$, or CH_2Br_2) intercalated between the 2D oxalate network. The magnetic properties and Mössbauer spectroscopy indicate that they undergo long-range ferromagnetic ordering at 5.6 K and a spin crossover of the intercalated $[Fe(sal_2\text{-trien})]^+$ complexes at different temperatures $T_{1/2}$. The three compounds present a LIESST effect with a relaxation temperature T_{LIESST} inversely proportional to $T_{1/2}$. The isostructural paramagnetic compound, $[Fe^{III}(sal_2\text{-trien})][Zn^{II}Cr^{III}(ox)_3]\cdot CH_2Cl_2$ (**2·CH$_2$Cl$_2$**) was also prepared. This compound presents a partial spin crossover of the inserted Fe^{III} complex as well as a LIESST effect. Finally, spectroscopic characterization of the Fe^{III} doped compound $[Ga_{0.99}Fe_{0.01}(sal_2trien)][Mn^{II}Cr^{III}(ox)_3]\cdot CH_2Cl_2$ (**3·CH$_2$Cl$_2$**) shows a gradual and complete thermal spin crossover and a LIESST effect on the isolated Fe^{III} complexes. This result confirms that cooperativity is not a necessary condition to observe the LIESST effect in an Fe^{III} compound.

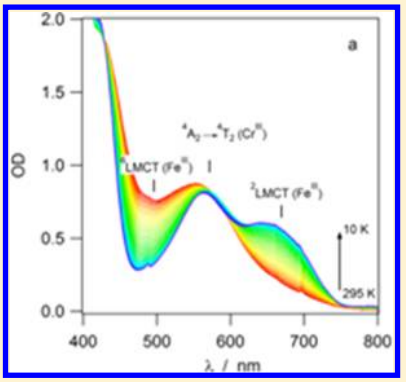

INTRODUCTION

Multifunctionality is one of the most appealing topics in chemical science. A rational approach to design multifunctional materials consists of creating hybrid solids constituted of two networks formed by two molecular fragments, where each network furnishes distinct physical properties.[1] A coexistence of the two physical properties is anticipated if the two networks are quasi-independent. Materials for which physical properties can be tuned by applying an external stimulus are attracting considerable interest in view of their potential applications as chemical switches, memories, or molecular sensors.[2] Most of the responsive magnetic materials obtained so far are one-network materials in which the magnetic order is tuned by light or pressure.[3] Two-network materials formed by a magnetic lattice and a switchable molecular component are promising candidates for the preparation of multifunctional responsive materials.

A potential source for this type of materials is the bimetallic oxalate-bridged complexes that have provided remarkable examples of multifunctional magnetic materials.[4] An interesting example prepared by our group is the compound $[Fe^{III}(sal_2\text{-trien})][Mn^{II}Cr^{III}(ox)_3]\cdot CH_2Cl_2$ (**1·CH$_2$Cl$_2$**, H_2sal_2-trien = *N*,*N*′-disalicylidenetriethylene-tetramine, ox = oxalate).[5] This compound shows an unusual combination of properties in the same compound; a spin crossover (SCO) transition of the inserted complex cation and a ferromagnetic ordering of the oxalate network. Unfortunately, no interplay between these two properties has been detected due to the large difference in temperature at which the two phenomena occur. Thus, while the SCO occurs at comparatively high temperatures, that is, in the range of 130−350 K, the ferromagnetic ordering occurs below 5.2−5.6 K. A way to overcome this limitation is to take advantage of the photoinduced SCO effect, also known as light-induced excited spin-state trapping (LIESST) effect originally established for Fe^{II} complexes at temperatures typically below 50 K.[6] Light irradiation at low temperatures, induces a LIESST effect for **1·CH$_2$Cl$_2$** with a T(LIESST) = 41 K, which defines the limiting temperature above which the photoinscribed information is erased.[7] The photoinduced spin conversion of the inserted Fe^{III} complex, however, has a negligible influence on the magnetic behavior of the 2D oxalate network. This is

Received: March 15, 2013
Published: May 15, 2013

   dx.doi.org/10.1021/ja402674x | J. Am. Chem. Soc. 2013, 135, 8655−8667

Table 1a. Crystallographic Data for Compounds 1·$CHCl_3$, 1·$CHBr_3$, and 1·CH_2Br_2 at 100 K and 2·CH_2Cl_2 at 120 K

compound	1·$CHCl_3$	1·$CHBr_3$	1·CH_2Br_2	2·CH_2Cl_2
empirical formula	$C_{27}H_{25}Cl_3CrFeMnN_4O_{14}$	$C_{27}H_{25}Br_3CrFeMnN_4O_{14}$	$C_{27}H_{26}Br_2CrFeMnN_4O_{14}$	$C_{27}H_{26}Cl_2CrFeZnN_4O_{14}$
formula weight	898.65	1032.03	953.13	874.64
crystal color	brown	brown	brown	brown
temperature (K)	100	100	100	120
wavelength (Å)	0.71073	0.71073	0.71073	0.71073
crystal system, Z	monoclinic, 4	monoclinic, 4	monoclinic, 4	monoclinic, 4
space group	$P2_1/c$	$P2_1/c$	$P2_1/c$	$P2_1/c$
a (Å)	11.7374(14)	11.9224(5)	11.7115(4)	11.6634(6)
b (Å)	31.6700(30)	31.8487(8)	31.9453(7)	31.4028(11)
c (Å)	9.5800(9)	9.6032(3)	9.5068(3)	9.3270(4)
β (°)	111.136(12)	110.582(4)	109.821(4)	109.747(5)
V (Å^3)	3321.5(6)	3413.7(2)	3346.04(17)	3215.2(2)
ρcalc (Mg/m^3)	1.797	2.008	1.892	1.807
μ(MoKα) (mm^{-1})	1.443	4.681	3.580	1.760
θ range (°)	2.98−28.30	2.97−30.56	2.97−30.49	2.26−32.51
reflns collected	8291	10 433	10 248	10 735
independent reflns, n, (R_{int})	2839 (0.1888)	7423 (0.1048)	8128 (0.0696)	3454 (0.1214)
L. S. parameters/restraints	325/0	460/0	451/0	421/0
$R1(F)$,[a] $I > 2\sigma(I)$]	0.0481	0.0608	0.0545	0.0493
$wR2(F^2)$,[b] all data	0.0813	0.1425	0.1098	0.0867
$S(F^2)$,[c] all data	0.638	1.061	1.176	0.665

[a] $R1(F) = \sum(|F_o| - |F_c|)/\sum|F_o|$. [b] $wR2(F^2) = [\sum w(F_o^2 - F_c^2)^2/\sum wF_o^4]^{1/2}$. [c] $S(F^2) = [\sum w(F_o^2 - F_c^2)^2/(n-p)]^{1/2}$.

not unexpected, as 2D oxalate networks with very different interlayer separations present a similar behavior.

Although the preparation of a switchable magnet has not been achieved, the LIESST effect of this compound constitutes a remarkable finding, as this phenomenon is rarely observed in Fe^{III} complexes. SCO Fe^{II} compounds present an average bond length change of about 0.20 Å between the LS and HS states, whereas that of Fe^{III} SCO complexes is about 0.13 Å. Obviously, the structural reorganization influences the kinetics of the spin-state interconversion. It is presumed that the lifetime of the photoinduced excited HS state for Fe^{III} complexes is shorter than that for Fe^{II} complexes, as the smaller energy barrier between the HS and LS states in Fe^{III} complexes cannot prevent the relaxation of the metastable HS state back to the LS ground state effectively. Only a few examples of Fe^{III} complexes showing the LIESST effect have been reported by Sato, Hayami et al., namely $[Fe^{III}(pap)_2]^+$, $[Fe^{III}(qsal)_2]^+$, and $[Fe^{III}(qnal)_2]^+$ (Hpap =2-(2-pyridilmethylamino)phenol, Hqsal =2-[(8-quinolinylimino)-mehyl]phenol, and Hqnal =1-((8-quinolinylimino)methyl)-2-naphthalenol).[8−10] The LIESST effect of these compounds is attributed to the strong distortion of the Fe^{III} sites from their octahedral geometry, which is enhanced by the presence of strong intermolecular interactions, such as $\pi-\pi$ stacking.[9] In contrast to the above Fe^{III} complexes in the form of salts of small anions, such as BF_4^- or ClO_4^-, **1·CH_2Cl_2** presents an extended 2D anionic network formed by Mn^{II} and Cr^{III} ions linked through oxalate ligands. $[Fe^{III}(sal_2\text{-trien})]^+$ cations and CH_2Cl_2 solvent molecules are intercalated between these oxalate layers.[5] Besides **1·CH_2Cl_2**, other compounds formed by the insertion of $[Fe^{III}(sal_2\text{-trien})]^+$ or $[Fe^{III}(X\text{-}sal_2\text{-trien})]^+$ (X = 5-Cl, 5-Br, 5-NO_2, 5-CH_3O, 4-Br, 3-Br, 3-Cl, and 3-CH_3O) into 2D or 3D bimetallic oxalate networks have been prepared by us,[5,11] but the LIESST effect has so far only been observed in **1·CH_2Cl_2**.[7]

In this work, a family of compounds with a similar structure to that of **1·CH_2Cl_2** has been prepared by replacing CH_2Cl_2 with other halogenated solvents. Furthermore, a fraction of the Fe^{III} SCO complexes of **1·CH_2Cl_2** has been replaced with the diamagnetic dopant, $[Ga^{III}(sal_2\text{-trien})]^+$ complex, to prepare compounds of formula $[Ga^{III}_{1-x}Fe^{III}_x(sal_2\text{-trien})]$-$[Mn^{II}Cr^{III}(ox)_3]\cdot CH_2Cl_2$. The aim of this work is to obtain new Fe^{III} compounds presenting a LIESST effect that could provide more data to understand this rare property. On the other hand, substitution of the solvent molecule may allow tuning the temperatures of the thermal and photoinduced SCO of the inserted Fe^{III} cations. We have to take into account that replacement of the solvent molecules induces changes in the internal chemical pressure of the inserted Fe^{III} SCO complex and in the intermolecular interactions with the oxalate network, that are key factors for the SCO properties. Finally, dilution of the $[Fe^{III}(sal_2\text{-trien})]^+$ complex with an inert $[Ga^{III}(sal_2\text{-trien})]^+$ complex reduces cooperativity and may help to clarify the role of intermolecular interactions between SCO complexes in this type of compound. An additional advantage of dilution is that it permits to perform spectroscopic characterization on single crystals, which is not possible for pure Fe^{III} compounds due to the strong absorption of $[Fe^{III}(sal_2\text{-trien})]^+$ complexes.

EXPERIMENTAL SECTION

Synthesis. $[Fe(sal_2\text{-trien})]PF_6$ and $[Ga(sal_2\text{-trien})]PF_6$ were prepared according to literature methods.[12] $Ag_3[Cr(ox)_3]$ was prepared by metathesis from the corresponding potassium salt.[13] All other materials and solvents were commercially available and used without further purification. Single crystals of the five compounds $[Fe^{III}(sal_2\text{-trien})][Mn^{II}Cr^{III}(ox)_3]\cdot CHCl_3$ (**1·$CHCl_3$**), $[Fe^{III}(sal_2\text{-trien})][Mn^{II}Cr^{III}(ox)_3]\cdot CHBr_3$ (**1·$CHBr_3$**), $[Fe^{III}(sal_2\text{-trien})]$-$[Mn^{II}Cr^{III}(ox)_3]\cdot CH_2Br_2$ (**1·CH_2Br_2**), $[Fe^{III}(sal_2\text{-trien})]$-$[Zn^{II}Cr^{III}(ox)_3]\cdot CH_2Cl_2$ (**2·CH_2Cl_2**), and $[Ga^{III}_{1-x}Fe^{III}_x(sal_2\text{-trien})]$-$[Mn^{II}Cr^{III}(ox)_3]\cdot CH_2Cl_2$ (**3·CH_2Cl_2**, x = 0.01) were obtained by slow diffusion of two solutions. The first solution was prepared by adding $MnCl_2\cdot 4H_2O$ (0.040 g, 0.202 mmol for **1·$CHBr_3$**, **1·$CHCl_3$**, and **1·CH_2Br_2**) or $ZnCl_2$ (0.075 g, 0.536 mmol for **2·CH_2Cl_2**) to a suspension of $Ag_3Cr(ox)_3$ (0.086 g, 0.134 mmol) in 9 mL of methanol. The AgCl precipitate was filtered. The second solution was obtained

dx.doi.org/10.1021/ja402674x | J. Am. Chem. Soc. 2013, 135, 8655−8667

Table 1b. Crystallographic Data for Compounds 1·$CHCl_3$, 1·$CHBr_3$, 1·CH_2Br_2, and 3·CH_2Cl_2 at 300 K

compound	1·$CHCl_3$	1·$CHBr_3$	1·CH_2Br_2	3·CH_2Cl_2
empirical formula	$C_{27}H_{25}Cl_3CrFeMnN_4O_{14}$	$C_{27}H_{25}Br_3CrFeMnN_4O_{14}$	$C_{27}H_{26}Br_2CrFeMnN_4O_{14}$	$C_{27}H_{26}Cl_2CrGaMnN_4O_{14}$
formula weight	898.65	1032.03	953.13	878.08
crystal color	brown	brown	brown	brown
temperature (K)	300	300	300	300
wavelength (Å)	0.71073	0.71073	0.71073	0.71073
crystal system, Z	monoclinic, 4	monoclinic, 4	monoclinic, 4	monoclinic, 4
space group	$P2_1/c$	$P2_1/c$	$P2_1/c$	$P2_1/c$
a (Å)	12.1519(17)	12.2769(4)	12.1735(6)	12.0528(9)
b (Å)	31.939(4)	32.0813(8)	32.3048(9)	32.1554(15)
c (Å)	9.4867(12)	9.5335(3)	9.4392(4)	9.4707(6)
β (°)	111.480(15)	110.849(4)	111.274(5)	112.297(8)
V (Å^3)	3426.2(8)	3508.99(18)	3459.1(2)	3396.0(4)
ρcalc (Mg/m^3)	1.742	1.954	1.830	1.717
μ(MoKα) (mm^{-1})	1.399	4.5554	3.463	8.594
θ range (°)	2.99−28.27	2.97−30.48	2.98−30.47	2.75−75.29
reflns collected	8222	10 725	10 590	6650
independent reflns, n, (R_{int})	1757 (0.2370)	5973 (0.1012)	4921 (0.1229)	4235 (0.0541)
L. S. parameters/restraints	252/0	497/0	461/0	489/0
$R1(F)$,[a] $I > 2\sigma(I)$]	0.0510	0.0649	0.0794	0.0709
$wR2(F^2)$,[b] all data	0.1078	0.1701	0.2291	0.2248
$S(F^2)$,[c] all data	0.577	1.030	1.025	1.074

[a] $R1(F) = \sum(|F_o| - |F_c|)/\sum|F_o|$. [b] $wR2(F^2) = [\sum w(F_o^2 - F_c^2)^2/\sum wF_o^4]^{1/2}$. [c] $S(F^2) = [\sum w(F_o^2 - F_c^2)^2/(n-p)]^{1/2}$.

by dissolving [Fe(sal$_2$-trien)]PF_6 (0.075 g, 0.134 mmol) in 9 mL of chloroform (**1·$CHCl_3$**), bromoform (**1·$CHBr_3$**), dibromomethane (**1·CH_2Br_2**), and dichloromethane (**2·CH_2Cl_2**) or a mixture of 0.1 and 9.9 mL of 15 mM solutions of [Fe(sal$_2$-trien)]PF_6 and [Ga(sal$_2$-trien)]PF_6, respectively, in dichloromethane (**3·CH_2Cl_2**). After two weeks brown or violet (**3·CH_2Cl_2**) crystals were obtained.

Structural Characterization. Single crystals of all five compounds were mounted on glass fibers using a viscous hydrocarbon oil to coat the crystal and then transferred directly to the cold nitrogen stream for data collection. X-ray data were collected at 100 and 300 K for **1·$CHCl_3$**, **1·$CHBr_3$** and **1·CH_2Br_2**, at 120 K for **2·CH_2Cl_2**, and at 300 K for **3·CH_2Cl_2** on a diffractometer equipped with a graphite-monochromated Enhance (Mo) X-ray Source (λ = 0.71073 Å). The program CrysAlisPro, Oxford Diffraction Ltd., was used for unit cell determinations and data reduction. Empirical absorption correction was performed using spherical harmonics, implemented in the SCALE3 ABSPACK scaling algorithm. Crystal structures were solved by direct methods with the SIR97 program[14] and refined against all F^2 values with the SHELXL-97 program,[15] using the WinGX graphical user interface.[16] Non-hydrogen atoms were refined anisotropically (except as noted), and hydrogen atoms were placed in calculated positions refined using idealized geometries (riding model) and assigned fixed isotropic displacement parameters. In compound **1·$CHCl_3$**, the small size of the crystals gave rise to a very weak scattering. Due to this, the number of reflections was not enough to carry out anisotropic refinement of all the atoms. Thus, carbon atoms at 100 K and carbon, nitrogen, and oxygen atoms at 300 K could only be modeled isotropically. Furthermore, this caused a too low observed/unique reflections ratio in the structure solved at 300 K. This problem disappeared in the structure of the same crystal solved at 100 K. Data collection and refinement statistics are collected in Table 1a. CCDC-929201 to 929208 contain the supplementary crystallographic data for this paper. These data can be obtained free of charge from The Cambridge Crystallographic Data Centre via www.ccdc.cam.ac.uk/data_request/cif.

The 0.5 mm glass capillaries were filled with polycrystalline samples of **1·$CHCl_3$**, **1·$CHBr_3$**, and **1·CH_2Br_2** and mounted and aligned on a Empyrean PANalytical powder diffractometer, using CuKα radiation (λ = 1.54177 Å). A total of 2 scans were collected at room temperature in the 2θ range 5−30°.

Physical Measurements. Magnetic susceptibility measurements were performed on polycrystalline samples using a magnetometer (Quantum Design MPMS-XL-5) equipped with a SQUID sensor. Variable-temperature measurements were carried out in the temperature range 2−400 K. The ac measurements were performed in the temperature range 2−10 K at different frequencies with an oscillating magnetic field of 0.395 mT. The magnetization and hysteresis studies were performed between 5 and −5 T, cooling the samples at zero field. The Ga:Fe:M:Cr:X (M = Mn or Zn and X = Br or Cl) ratios were measured on a Philips ESEM X230 scanning electron microscope equipped with an EDAX DX-4 microprobe.

Mössbauer spectra were collected in transmission mode using a conventional constant-acceleration spectrometer and a 25 mCi ^{57}Co source in a Rh matrix. The velocity scale was calibrated using an α-Fe foil. The absorber was obtained by gently packing single crystals of **1·$CHCl_3$**, **1·$CHBr_3$**, and **1·CH_2Br_2** into a perspex holder. Low-temperature spectra were collected using a bath cryostat with the sample immersed in liquid He for measurements at 4.2 K or by using flowing He gas to cool the sample above 4.2 K (temperature stability of 0.5 K). The spectra were fitted to Lorentzian lines using a nonlinear least-squares method.[17] Isomer shifts are given relative to metallic α-Fe at room temperature.

Variable-temperature optical single crystal absorption spectra of **3·CH_2Cl_2** were recorded with a commercial double beam spectrometer (Varian, Cary 5000). To this end a small crystal was mounted with silver paste so as to cover an aperture on a copper sample holder, which in turn was mounted on the coldfinger of an optical close cycle cryostat (Janis, Sumitomo SHI-4.5) capable of achieving a base temperature of 4 K.

RESULTS

Synthesis. The method used to prepare the family of five compounds of the present work was described in the Experimental Section and is analogous to that used to prepare **1·CH_2Cl_2**.[5] In previous work, two different types of structures were obtained depending on the solvent used to dissolve-[Fe^{III}(sal$_2$-trien)]PF_6.[5] A 2D bimetallic oxalate network is obtained with CH_2Cl_2 in **1·CH_2Cl_2**, while a 3D bimetallic oxalate network is obtained with CH_3CN and CH_3NO_2. In this work, we have discovered that the halogenated solvents,

dx.doi.org/10.1021/ja402674x | J. Am. Chem. Soc. 2013, 135, 8655−8667

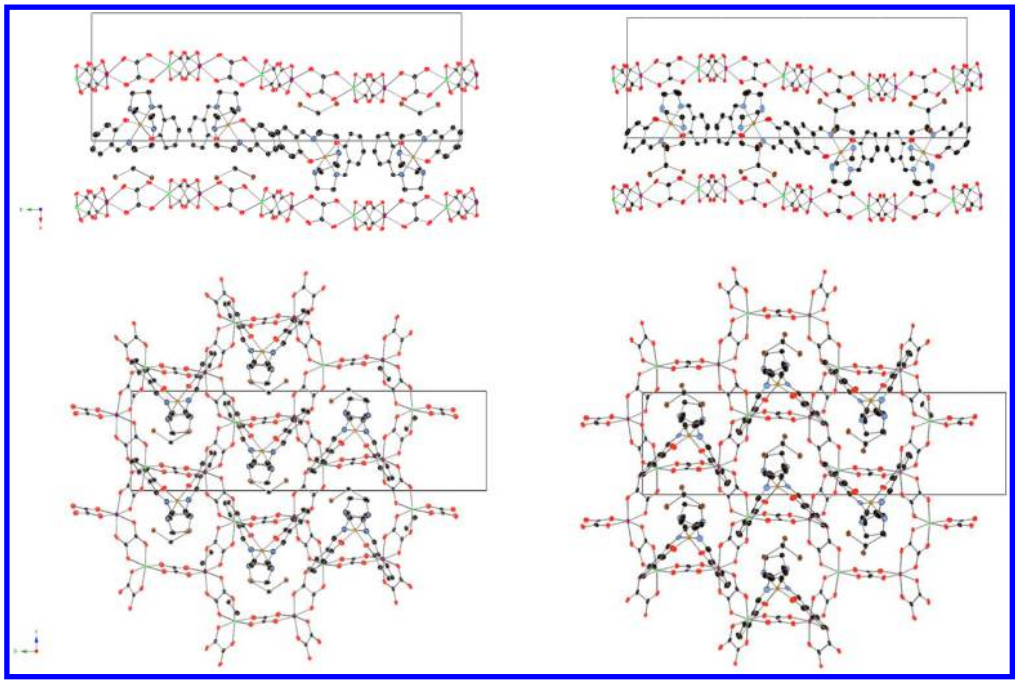

Figure 1. Projection on the *ab* (top) and *bc* (bottom) planes of the structures of **1·CH$_2$Br$_2$** (left) and **1·CHBr$_3$** (right) at 100 K; Mn (pink), Cr (green), Fe (yellow), C (black), N (blue), O (red), Br (brown). Neighboring atoms corresponding to disordered Mn/Cr have been assigned as Mn and Cr separately for clarity, and hydrogen atoms have been omitted for clarity.

$CHCl_3$, $CHBr_3$, and CH_2Br_2, give rise to 2D structures similar to that of **1·CH$_2$Cl$_2$**. This confirms that the formation of 2D or 3D networks is controlled by the size and configuration of the templating cation, which change in the different solvents. An interesting example of how subtle changes lead to 2D or 3D structures is the use of other $[M^{III}(sal_2\text{-trien})]^+$ complexes in the same solvent (CH_2Cl_2). Thus, the largest cation, $[In^{III}(sal_2\text{-trien})]^+$, gives rise to a 3D structure,[18] while the smallest one, $[Ga^{III}(sal_2\text{-trien})]^+$,[19] leads to a 2D one. Therefore, the halogenated solvents, CH_2Cl_2, CH_2Br_2, $CHCl_3$, and $CHBr_3$, lead to 2D structures with $[Fe^{III}(sal_2\text{-trien})]^+$ because they induce a configuration of the cation suitable for the growth of the 2D network, which is also stabilized by the insertion of the solvent molecules. When a similar cation of larger size, such as $[In^{III}(sal_2\text{-trien})]^+$, is used, the 3D network is favored, and the solvent molecules do not enter the structure. This allows preparing 2D compounds containing two different cations of similar size and to dilute the SCO Fe^{III} complexes with diamagnetic Ga^{III} complexes. In the compounds of formula $[Ga^{III}_{1-x}Fe^{III}_x(sal_2\text{-trien})][Mn^{II}Cr^{III}(ox)_3]\cdot CH_2Cl_2$, most of the $[Fe^{III}(sal_2\text{-trien})]^+$ complexes of **1·CH$_2$Cl$_2$** are replaced by the diamagnetic $[Ga^{III}(sal_2\text{-trien})]^+$ complexes. They are prepared by mixing the $[Ga^{III}(sal_2\text{-trien})]PF_6$ and $[Fe^{III}(sal_2\text{-trien})]PF_6$ precursors in the desired ratio.

The composition of the compounds was checked by microanalysis, which shows the presence of the solvent molecules in the structures. Thus, a 1:1:1:3 Fe:M(Mn or Zn):Cr:X(X = Cl or Br) ratio was found for **1·CHCl$_3$** and **1·CHBr$_3$**, while a 1:1:1:2 ratio is found for **1·CH$_2$Br$_2$** and **2·CH$_2$Cl$_2$**. The Ga:Fe ratio for $[Ga^{III}_{1-x}Fe^{III}_x(sal_2\text{-trien})][Mn^{II}Cr^{III}(ox)_3]\cdot CH_2Cl_2$ was found to be close to the ratio of the solutions used in the synthesis. For the lightly doped compound $[Ga^{III}_{1-x}Fe^{III}_x(sal_2\text{-trien})][Mn^{II}Cr^{III}(ox)_3]\cdot CH_2Cl_2$, ($x$ = 0.01, **3·CH$_2$Cl$_2$**) used for optical spectroscopic characterization, the iron content was found to be <1% and could not determined accurately. Still, the presence of Fe in the single crystals of **3·CH$_2$Cl$_2$** is verified by the presence of the characteristic LMCT bands in the absorption spectrum (see below).

Structure. The single crystal X-ray diffraction study of **1·CHCl$_3$**, **1·CHBr$_3$**, **1·CH$_2$Br$_2$**, **2·CH$_2$Cl$_2$**, and **3·CH$_2$Cl$_2$** shows that they present very similar structures to that of **1·CH$_2$Cl$_2$**. Indeed, their unit cell parameters are very close to the one of **1·CH$_2$Cl$_2$** (see Table 1b). The structures of **1·CHCl$_3$**, **1·CHBr$_3$**, and **1·CH$_2$Br$_2$** were solved at 100 and 300 K, as at these temperatures the Fe^{III} complexes are close to 100% in the LS or the HS state, respectively. On the other hand, the structure of **2·CH$_2$Cl$_2$** could only be solved at 120 K due to the lower quality of the crystals and the only partial SCO exhibited by this compound (see below). Finally, powder X-ray diffraction patterns of **1·CHCl$_3$**, **1·CHBr$_3$**, and **1·CH$_2$Br$_2$** at 300 K confirm the structure obtained from single X-ray diffraction experiments (see Figure S1).

As in the case of **1·CH$_2$Cl$_2$**, the four compounds are formed by anionic $[M^{II}Cr^{III}(ox)_3]^-$ (M = Mn or Zn) sheets in the *bc* plane alternating with interlamellar $[Fe^{III}(sal_2\text{-trien})]^+$ cationic complexes and solvent molecules (see Figure 1). The anionic layers present a 2D honeycomb structure with two crystallographically independent metals linked through oxalate ligands. The intermediate metal−oxygen distances with respect to the ones expected for Cr^{III}−O and Mn^{II}−O (Zn^{II}−O for **2·CH$_2$Cl$_2$**) do not allow distinguishing between the two metals in these structures. The cationic layer contains one crystallographically independent $[Fe^{III}(sal_2\text{-trien})]^+$ (or $[Ga^{III}(sal_2\text{-trien})]^+$ in **3·CH$_2$Cl$_2$**) complex and one solvent molecule (CH_2Cl_2, $CHCl_3$, $CHBr_3$ or CH_2Br_2).

We will now focus on the differences between the crystal structures measured at 100 and 300 K as they may help to understand the structural changes associated with the SCO. Furthermore, they will be compared with those observed in **1·CH$_2$Cl$_2$**. We will look first at the usual changes in the

dx.doi.org/10.1021/ja402674x | J. Am. Chem. Soc. 2013, 135, 8655−8667

Table 2. Structural Parameters of 1·$CHCl_3$, 1·$CHBr_3$, 1·CH_2Br_2, and 2·CH_2Cl_2

	spin state	mean Fe−N (Å)	mean Fe−O (Å)	N(amine)−Fe−O(Phenoxo) (°)	N(imine)−Fe−N(imine) (°)
1·$CHCl_3$ (300 K)	100% HS	2.142(5)	1.905(5)	156.9(2) and 157.9(2)	177.2(2)
1·$CHCl_3$ (100 K)	~5% HS	1.985(4)	1.865(3)	171.86(15) and 170.75(15)	178.72(16)
1·$CHBr_3$ (300 K)	100% HS	2.148(5)	1.897(4)	156.2(2) and 156.73(2)	176.7(2)
1·$CHBr_3$ (100 K)	~25% HS	2.013(5)	1.875(4)	168.5(2) and 167.45(19)	177.90(19)
1·CH_2Br_2 (300 K)	100% HS	2.135(6)	1.885(6)	158.1(3) and 160.1(2)	176.3(3)
1·CH_2Br_2 (100 K)	100% LS	1.982(3)	1.865(3)	173.49(14) and 173.17(13)	179.14(15)
2·CH_2Cl_2 (120 K)	100% LS	1.969(4)	1.857(3)	172.99(14) and 173.47(14)	178.91(16)

coordination geometry of the Fe^{III} complex between the LS and HS states (Fe−N or Fe−O bond lengths and distortions from the octahedral geometry) and then at the differences in crystal packing.

The first effect of lowering the temperature is a shortening on metal−ligand bond lengths (see Table 2), which is similar to that found for **1·CH_2Cl_2** (average bond length differences of Δr_{HL}(Fe−N) = 0.149 Å and Δr_{HL}(Fe−O) = 0.024 Å).[7] The small variation in these values between the different compounds may be attributed to a different fraction of Fe^{III} complexes undergoing SCO from 300 to 100 K.

The second difference concerns the distortion of the octahedral coordination site, which is larger for the HS state as observed in **1·CH_2Cl_2**.[7] Thus, at 300 K the angles of two of the three diagonals from the octahedron, defined by the bonds N(amine)−Fe−O(phenoxo), N(amine) = N2, N3, differ strongly from 180°, while the remaining one, defined by the bond N(imine)−Fe−N(imine), N(imine) = N1, N4, is closer to 180°. The coordination octahedron is much more regular at 100 K with angles of all three diagonals closer to 180° (see Table 2).

The third difference between the LS and HS structures is related to the disorder of the ethylene groups of [Fe(sal_2-trien)]$^+$ and solvent molecules. At 300 K, two of the three ethylene groups of [Fe(sal_2-trien)]$^+$ in **1·$CHBr_3$** and **1·$CHCl_3$** and the three of them in **1·CH_2Br_2** present a disorder, which has been solved by considering two possible configurations with occupancies of 62 and 38% for **1·$CHBr_3$**, 69 and 31% for **1·$CHCl_3$**, and 63 and 37% for **1·CH_2Br_2**. This disorder is not observed in the structures of these compounds solved at 100 K. This disorder could be related to the presence of HS Fe^{III} complexes as it disappears at low temperatures, where Fe is in the LS state. On the other hand, in **1·CH_2Br_2** one over the two Br atoms of the CH_2Br_2 solvent presents a disorder at 300 K that could be solved assuming two possible configurations with occupancies of 85 and 15%. This disorder disappears at 100 K. **1·CH_2Cl_2** presents a similar disorder in the ethylene groups and in the Cl atoms of CH_2Cl_2 molecules at 250 and 300 K, which disappears below 180 K.[7] This disorder is not present for $CHBr_3$ or $CHCl_3$ solvent molecules in **1·$CHCl_3$** and **1·$CHBr_3$**.

Finally, the crystal packing of [Fe^{III}(sal_2-trien)]$^+$ complexes in the four neat compounds also presents important differences between low and high temperature structures. As in the case of **1·CH_2Cl_2**, the *a* parameter, which gives the interlayer separation, decreases with the temperature (see Tables 1a and 1b). Therefore, the SCO from HS to LS states leads to a decrease of the interlayer separation. This shortening results in contacts between O atoms from oxalate layers and CH or CH_2 groups from [Fe^{III}(sal_2-trien)]$^+$, which are shorter at 100 K than at 300 K. Therefore, stronger interactions with the oxalate network are expected when the Fe^{III} complexes are in the LS state (see Tables S1−S6). On the other hand, interlayer distances of **1·CH_2Cl_2** are shorter than those of **1·$CHCl_3$**, **1·$CHBr_3$**, and **1·CH_2Br_2** (11.5602(4) Å at 92 K and 12.096(5) Å at 300 K for **1·CH_2Cl_2**)[7] at the same temperatures. Two factors could explain these differences: the change of CH_2Cl_2 by the more voluminous $CHCl_3$, $CHBr_3$ or CH_2Br_2 solvents and a different fraction of [Fe^{III}(sal_2-trien)]$^+$ in the HS state. Thus, at low temperatures, when almost 100% of Fe^{III} is in the LS state, a comparison of the *a* parameter for **1·$CHCl_3$** and **1·CH_2Br_2** at 100 K with that of **1·CH_2Cl_2** at 92 K demonstrates that the interlayer distance increases with the volume of the solvent. In the case of **1·$CHBr_3$**, ~25% of Fe^{III} is in the HS state at this temperature (see Mössbauer data below). This may be an additional factor contributing to the increase in interlayer separation. This indicates that the internal pressure on the inserted [Fe^{III}(sal_2-trien)]$^+$ complexes decreases as the size of the solvent increases. This could explain the stabilization of the HS state in the presence of the bulkier solvents. Magnetic measurements and Mössbauer spectra are consistent with this feature (see below).

Magnetic Properties. The thermal dependence of the product of the molar magnetic susceptibility times the temperature (χ_MT) of the three compounds is shown in Figure 2. The values for χ_MT are 10.9, 10.1, and 9.9 $cm^3 \cdot K \cdot mol^{-1}$ at

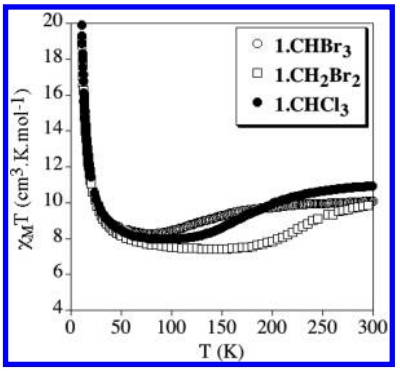

Figure 2. Temperature dependence of the product of the molar magnetic susceptibility with temperature (χ_MT) at 0.1 T for compounds **1·$CHCl_3$** (filled circles), **1·$CHBr_3$** (open circles), and **1·CH_2Br_2** (open squares).

300 K for **1·$CHCl_3$**, **1·$CHBr_3$**, and **1·CH_2Br_2**, respectively. These values are close to the sum of the expected contributions for the isolated paramagnetic ions with most of the Fe^{III} spin-crossover complexes in the HS state. The lower χ_MT values of **1·$CHBr_3$** and **1·CH_2Br_2** with respect of that of **1·$CHCl_3$** indicate that in these two compounds there is still a small Fe^{III} LS fraction at 300 K. This is consistent with Mössbauer data at 250 K (see below and Table 3). χ_MT decreases gradually in the three compounds from 300 K to reach minimum values at 140 K for **1·CH_2Br_2**, 95 K for **1·$CHCl_3$**, and 80 K for **1·$CHBr_3$**. Mössbauer data (see below) indicate that almost

dx.doi.org/10.1021/ja402674x | J. Am. Chem. Soc. 2013, 135, 8655−8667

Table 3. Estimated Parameters from the Mössbauer Spectra of 1·$CHCl_3$, 1·$CHBr_3$, and 1·CH_2Br_2[a]

compound	T		IS	QS	I
1·$CHCl_3$	250 K	Fe LS	0.12	2.35	10%
		Fe HS	0.30	0.18	90%
	230 K	Fe LS	0.14	2.43	17%
		Fe HS	0.29	0.21	83%
	220 K	Fe LS	0.15	2.43	26%
		Fe HS	0.29	0.2	74%
	175 K	Fe LS	0.19	2.50	54%
		Fe HS	0.30	0.2	46%
	150 K	Fe LS	0.20	2.54	77%
		Fe HS	0.28	0.20	22%
	100 K	Fe LS	0.21	2.52	93%
		Fe HS	0.33	0.40	7%
	80 K	Fe LS	0.21	2.54	95%
		Fe HS	0.27	0.34	5%
	4 K	Fe LS	0.21	2.45	100%
1·$CHBr_3$	250 K	Fe LS	0.14	2.35	15%
		Fe HS	0.36	0.34	85%
	230 K	Fe LS	0.15	2.40	22%
		Fe HS	0.36	0.40	78%
	210 K	Fe LS	0.16	2.50	27%
		Fe HS	0.36	0.41	73%
	190 K	Fe LS	0.17	2.56	28%
		Fe HS	0.37	0.40	72%
	170 K	Fe LS	0.18	2.59	34%
		Fe HS	0.36	0.35	66%
	130 K	Fe LS	0.20	2.57	57%
		Fe HS	0.36	0.31	43%
	100 K	Fe LS	0.20	2.56	72%
		Fe HS	0.36	0.35	28%
	77 K	Fe LS	0.21	2.59	82%
		Fe HS	0.37	0.44	18%
	4 K	Fe LS	0.22	2.61	100%
1·CH_2Br_2	245 K	Fe LS	0.15	2.53	28%
		Fe HS	0.32	–	72%
	199 K	Fe LS	0.16	2.52	78%
		Fe HS	0.34	0.46	22%
	180 K	Fe LS	0.18	2.57	85%
		Fe HS	0.34	0.49	15%
	160 K	Fe LS	0.19	2.60	90%
		Fe HS	0.35	0.49	10%
	77 K	Fe LS	0.20	2.56	100%
	63 K	Fe LS	0.21	2.60	100%
	4 K	Fe LS	0.21	2.61	100%

[a]IS is isomer shift relative to metallic Fe at 295 K; QS is quadrupole splitting; and I is relative area. Estimated errors are <0.03 mm/s for IS and QS and <2% for I.

100% of Fe^{III} is in the LS state below 80 K for **1·CH_2Br_2** and **1·$CHCl_3$**. In the case of **1·$CHBr_3$** at 77 K, there is still a significant fraction of Fe^{III} in the HS state (~18%) that disappears at 4 K. Therefore, the three compounds undergo an almost complete SCO with different $T_{1/2}$ values ($T_{1/2}$ = temperature of 50% HS→LS spin conversion). These values, calculated from Mössbauer data, are 230 K for **1·CH_2Br_2**, 180 K for **1·$CHCl_3$**, and 140 K for **1·$CHBr_3$**. This confirms that the presence of bulkier solvent molecules shifts $T_{1/2}$ toward lower values due to the lowering of the chemical pressure on the inserted $[Fe^{III}(sal_2\text{-trien})]^+$ complexes. At lower temperatures $\chi_M T$ increases due to the ferromagnetic interactions between neighboring Mn^{II}–Cr^{III} magnetic ions as observed for **1·CH_2Cl_2** and other M^{II}–Cr^{III} 2D oxalate networks. The ac susceptibility measurements confirm the presence of long-range magnetic ordering and permit to determine precisely the critical temperatures (T_c). A maximum in the in-phase signal (χ_M') near T_c and an out-of-phase signal (χ_M'') that starts to appear at temperatures just below T_c is observed in the three compounds (Figure 3). From this data the T_c of the three compounds is 5.6

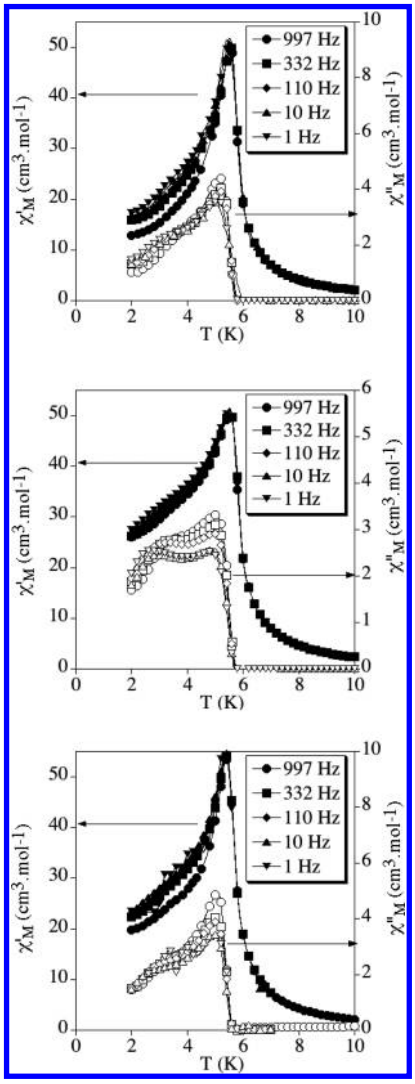

Figure 3. Temperature dependence of the in-phase ac susceptibility (χ') (filled symbols) and the out-of-phase ac susceptibility (χ'') (open symbols) for **1·$CHBr_3$** (top), **1·$CHCl_3$** (middle), and **1·CH_2Br_2** (bottom).

K, which is similar to that of **1·CH_2Cl_2** and other 2D Mn^{II}–Cr^{III} 2D oxalate compounds.[5,11a,c] These signals are frequency independent as expected for a ferromagnet.

Isothermal magnetization at 2 K of the three compounds shows the expected behavior for a ferromagnet (Figure S2). The magnetization (M) value at 5 T of the three compounds is 8.7 μ_B, which is close to the expected value of 9 μ_B for a parallel alignment of the spins in the bimetallic lattice with Fe^{III} in the LS state, thus confirming the complete HS→LS spin conversion at this temperature for the three compounds. The hysteresis loops at 2 K show that these compounds are soft

dx.doi.org/10.1021/ja402674x | J. Am. Chem. Soc. 2013, 135, 8655–8667

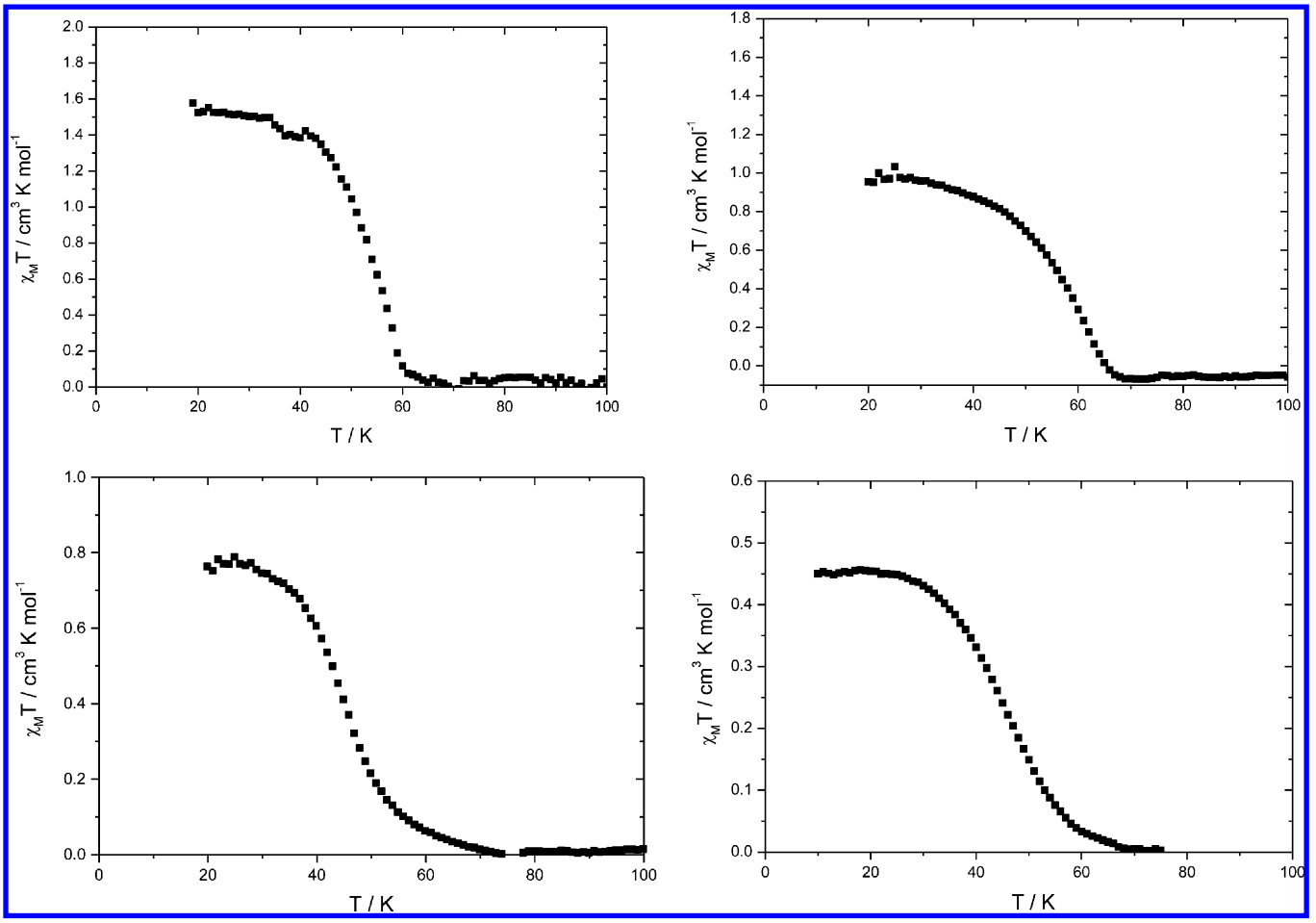

Figure 4. Difference between magnetic signal after and before photoconversion for compounds **1·CHCl$_3$** (top left), **1·CHBr$_3$** (top right), **1·CH$_2$Br$_2$** (bottom left), and **2·CH$_2$Cl$_2$** (bottom right).

ferromagnets with coercive fields of 3 mT for **1·CHBr$_3$** and 1 mT for **1·CH$_2$Br$_2$** and **1·CHCl$_3$**.

The temperature dependence of $\chi_M T$ for **2·CH$_2$Cl$_2$** is shown in Figure S3. $\chi_M T$ shows a value of 4.5 cm^3·K·mol^{-1} at 300 K. This value is approximately equal to the sum of the expected contributions for the isolated paramagnetic ions (Cr^{III} and Fe^{III}) with ca. 50% of the Fe^{III} spin-crossover complexes in a HS state. $\chi_M T$ decreases gradually from 300 to 150 K. Below this temperature, the decrease is less abrupt and reaches a plateau below 100 K with $\chi_M T$ values of 2.3 cm^3·K·mol^{-1} close to the expected value for isolated Cr^{III} ions and 100% of the Fe^{III} complexes in a LS state. Finally, below 10 K, there is a decrease of a $\chi_M T$ that can be due to spin−orbit coupling and zero-field splitting effects. These results demonstrate that inside the bimetallic oxalate framework the two metals are ordered in such a way that each Cr^{III} center is surrounded by three nonmagnetic Zn centers and that a 50% HS→LS spin conversion takes place from 300 to 100 K.

Photomagnetic Properties. **1·CHCl$_3$**, **1·CH$_2$Br$_2$**, **1·CHBr$_3$**, and **2·CH$_2$Cl$_2$** were introduced into SQUID at 10 K and irradiated with red light (λ = 647 nm). An increase of the magnetic signal was observed. After about 1 h, the irradiation was switched off. The temperature was then increased at a rate of 0.3 K min^{-1}, and the magnetic susceptibility recorded. For the four compounds, $\chi_M T$ recorded at low temperature after irradiation is higher than the value recorded in the dark. Upon increasing the temperature, the difference vanishes and becomes zero above a temperature between 60 and 80 K, depending on the compound. In order to see clearly the magnetic differences after and before irradiation, $\chi_M T$ after irradiation was subtracted to the one recorded before irradiation using an interpolation procedure. Interpolated differences are presented in Figure 4. At 20 K, the differences in $\chi_M T$ values are 1.5, 0.8, 1.0, and 0.45 cm^3·K·mol^{-1}, respectively, for **1·CHCl$_3$**, **1·CH$_2$Br$_2$**, **1·CHBr$_3$**, and **2·CH$_2$Cl$_2$**. Taking the mean values of 4.375 cm^3·K·mol^{-1} for Fe^{III} HS and 0.6 cm^3·K·mol^{-1} for Fe^{III} LS, the fraction of Fe^{III} photoconverted after irradiation is calculated to be 40, 21, 26, and 13% for **1·CHCl$_3$**, **1·CH$_2$Br$_2$**, **1·CHBr$_3$**, and **2·CH$_2$Cl$_2$**, respectively. As already described, the difference in $\chi_M T$ decreases when the temperature increases, being zero when the temperature is higher than 80 K. For the four compounds, T(LIESST) temperatures, defined as the minimum of the derivate of this $\chi_M T$ difference with regard to temperature, are respectively 58, 45, 62, and 45 K.

In order to get some insight into the decay of the photoinduced HS state, HS→LS relaxation curves were recorded for **1·CHCl$_3$**, **1·CH$_2$Br$_2$**, and **1·CHBr$_3$**. These are presented in Figure S4. For the three compounds, the relaxation curves show strong deviations from a single exponential in the shape of stretched exponentials. The best fit (solid lines in Figure S4) was obtained with a distribution of relaxation rate constants at a given temperature from a Gaussian distribution of activation energies as already observed

dx.doi.org/10.1021/ja402674x | J. Am. Chem. Soc. 2013, 135, 8655−8667

in **1·CH$_2$Cl$_2$**.[7] The apparent activation energy, E_a, apparent pre-exponential factor, k_∞, and standard deviation of the mean activation energy, σ, are reported in Table S7 for the three compounds. These curves are typical of noncooperative systems, which rarely show a single-exponential behavior, because of inhomogeneous distributions due to poorly crystalline solids and the presence of disorder.[20] Hence, in the present case the deviations could be related to the disorder observed in the ethylene groups of [Fe^{III}(sal$_2$-trien)]$^+$ in **1·CHCl$_3$**, **1·CH$_2$Br$_2$**, and **1·CHBr$_3$**, indicating different possible configurations of the cations in the HS state.

Mössbauer Spectroscopy. Mössbauer spectra of **1·CHCl$_3$**, **1·CH$_2$Br$_2$**, and **1·CHBr$_3$** shown in Figures 5, 6, and 7 are similar to those published for **1·CH$_2$Cl$_2$**, the achiral 3D compound [Fe^{III}(sal$_2$trien)][Mn^{II}Cr^{III}(ox)$_3$]·CH$_3$OH, or other compounds formed by the insertion of [Fe^{III}(5X-sal$_2$-trien)]$^+$ (X = Cl, Br) into chiral 3D oxalate networks.[5,11b] In the present compounds, only a quadrupole doublet with estimated parameters typical of LS Fe^{III} is observed at 4 K (Table 3). Above 77 K for **1·CHCl$_3$** and **1·CHBr$_3$** and 160 K for **1·CH$_2$Br$_2$**, an unresolved absorption, centered at IS ∼ 0.30−0.36 mm/s at 295 K, is observed. This broad absorption is assigned to HS Fe^{III}. As discussed in detail in previous papers,[5,11b] broadening of the HS Fe^{III} contribution below 180 K may hardly be attributed to a slow-spin state interconversion, since the LS Fe^{III} doublet peaks remain sharp with relatively thin line widths. In the 4−180 K temperature range broadening of the HS Fe^{III} seems to be rather due to slow relaxation of the HS Fe^{III} magnetic moments directions with a frequency (10^7−10^9 s^{-1}) whose reciprocal is of the same order of magnitude of the Mössbauer effect observation time. Below the temperatures referred to above, all the Fe centers are present as LS Fe^{III}, and therefore no sextets are observed at 4 K in contrast to [Fe(5-Cl-

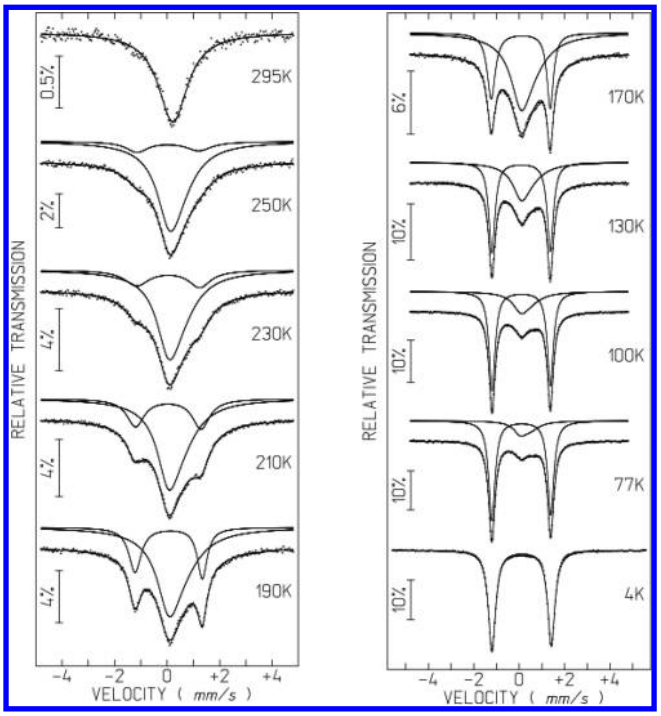

Figure 5. Mössbauer spectra of **1·CHBr$_3$** taken at different temperatures. The lines over the experimental points are the sum of two doublets corresponding to HS and LS Fe^{III}. The estimated parameters for these doublets are collected in Table 3.

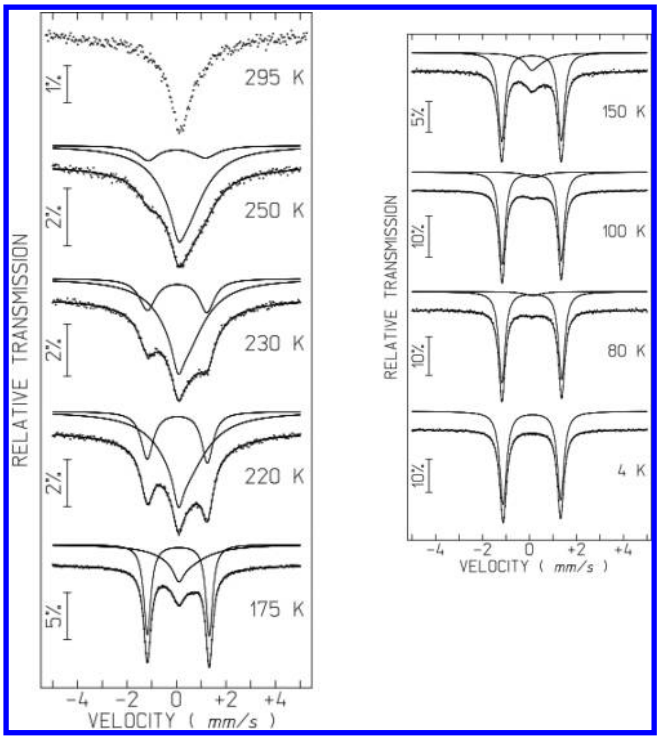

Figure 6. Mössbauer spectra of **1·CHCl$_3$** taken at different temperatures. The lines over the experimental points are the sum of two doublets corresponding to HS and LS Fe^{III}. The estimated parameters for these doublets are collected in Table 3.

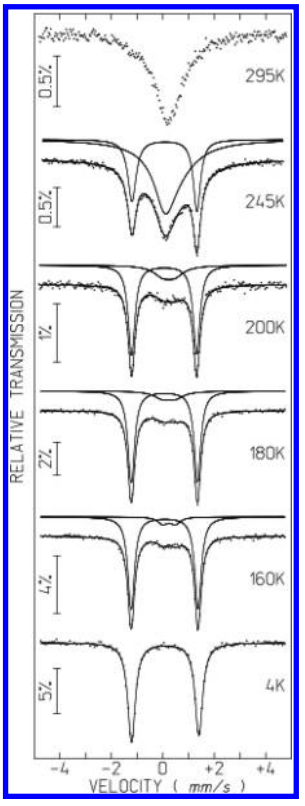

Figure 7. Mössbauer spectra of **1·CH$_2$Br$_2$** taken at different temperatures. The lines over the experimental points are the sum of two doublets corresponding to HS and LS Fe^{III}. The estimated parameters for these doublets are collected in Table 3.

dx.doi.org/10.1021/ja402674x | J. Am. Chem. Soc. 2013, 135, 8655−8667

$sal_2trien)][MnCr(ox)_3]\cdot 0.5CH_3NO_2$, $[Fe(5\text{-}Br\text{-}sal_2trien)][MnCr(ox)_3]$ and $[Fe(sal_2trien)][MnCr(ox)_3]\cdot CH_3OH$, where a significant fraction of Fe^{III} was still in the HS state at temperatures ≤4 K.[5,11b]

The temperature dependence of the estimated relative areas of the HS and LS Fe^{III} subspectra of the three compounds is plotted in Figure S5. They follow the same trend as the temperature dependence of $\chi_M T$ and permit to calculate the transition temperature $T_{1/2}$.

Spectroscopic Measurements on the Diluted System. The spin-crossover behavior of this family of Fe^{III} complexes has been studied by optical spectroscopy on single crystals. It is not possible to perform this type of measurements with the pure Fe compounds because the ligand−metal charge transfer (LMCT) absorption bands of the Fe complexes are very intense in the visible region and saturate the signal. Therefore, doped $[Ga^{III}_{1-x}Fe^{III}_x(sal_2\text{-}trien)][Mn^{II}Cr^{III}(ox)_3]\cdot CH_2Cl_2$ crystals were prepared. They show much less intense absorption bands, as Ga^{III} complexes do not absorb in the visible region of the spectrum. For good quality spectra, it was necessary to reduce the Fe content to 1 mol % (**3·CH$_2$Cl$_2$**).

Absorption spectra at different temperatures on a single crystal of **3·CH$_2$Cl$_2$** were recorded in order to follow the thermal SCO of the compound (Figure 8a). At room temperature, the characteristic LMCT band of the HS Fe^{III} complex is observed as a shoulder at around 500 nm of an intense band centered at 570 nm assigned to the spin allowed $^4A_2 \rightarrow {}^4T_2$ d−d transition of $[Cr(ox)_3]^{3-}$ of the bimetallic oxalate network. The latter practically does not change with temperature. Upon cooling, a band around 650 nm, due to an LMCT absorption of the LS complex, gradually appears and increases in intensity. At the same time, the intensity of the above-mentioned HS band decreases. The temperature dependence of the HS fraction was monitored by analyzing the evolution of the absorbance of the LMCT absorption bands. For a quantitative evaluation of the resultant thermal spin transition, the evolution of the optical density at 665 nm as a function of temperature has been normalized with the data from the magnetic measurements performed on **1·CH$_2$Cl$_2$**.[5] Comparison of this result with magnetic data of the pure Fe compound **1·CH$_2$Cl$_2$** is shown in Figure 8b. For both compounds a gradual variation of the HS fraction is observed, with an estimated HS fraction at room temperature of 80%. For the doped system **3·CH$_2$Cl$_2$**, $T_{1/2}$ is shifted to lower temperatures ($T_{1/2}$ = 225 K) compared to **1·CH$_2$Cl$_2$** ($T_{1/2}$ = 245 K).[7] Furthermore, the transition is more gradual in **3·CH$_2$Cl$_2$** than in the pure Fe compound **1·CH$_2$Cl$_2$**. This observation can be explained by the lack of cooperative interactions in lightly doped crystals.

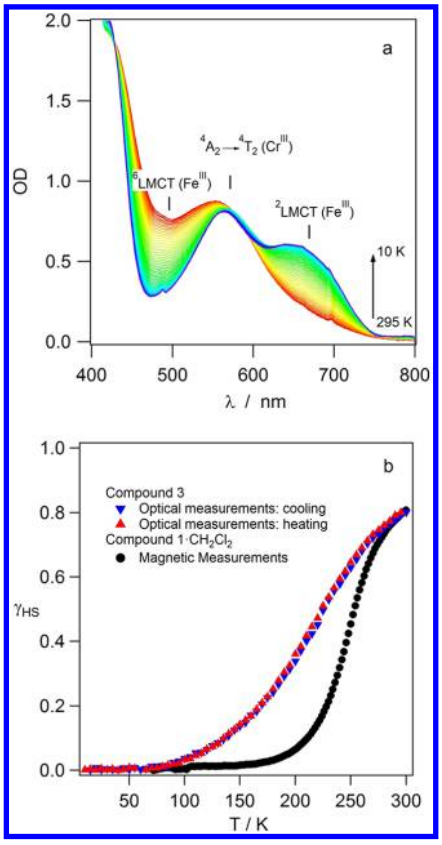

Figure 8. (a) Variable-temperature single crystal absorption spectra of **3·CH$_2$Cl$_2$**. (b) Thermal SCO for **3·CH$_2$Cl$_2$** extracted from spectroscopic measurements (red and blue triangles) and of **1·CH$_2$Cl$_2$** from magnetic measurements from reference 5 (black circles).

For LIESST experiments the sample was irradiated at 5 K with a continuous diode pumped solid-state laser at 690 nm. Irradiation at this wavelength, which is within the LMCT absorption of the LS species, resulted in a light-induced population of the metastable HS state at the expense of the LS state. Irradiation for only 2 min at 1 mW/mm^2 in fact resulted in an almost quantitative transformation from the LS state to the photoexcited HS state (Figure 9a), since the absorption spectrum of **3·CH$_2$Cl$_2$** in the photoexcited state at low temperature is almost identical to the one obtained at room temperature. Absorption spectra after photoexcitation were subsequently recorded between 5 and 70 K with a heating rate of 0.3 K/min. The HS fraction at every temperature was calculated from the evolution of the absorbance at 665 nm, taking the spectrum at 5 K as the LS reference and the one obtained just after irradiation at this temperature as the HS reference. The HS fraction remains close to 100% from 5 to 30 K. At higher temperatures it decreases to reach a value close to zero at around 60 K (Figure 9b). This gives a T(LIESST) of 43 K, which is similar to the result obtained from the magnetic measurements for the pure Fe compound **1·CH$_2$Cl$_2$**.[7] In contrast to the magnetic measurements on the pure Fe crystals, for which a light-induced HS fraction of only 0.4 could be achieved,[7] in the very dilute system it proved possible to achieve a quantitative population of the HS state. This is due to the comparatively weak optical density of the dilute crystals, which results in a good penetration and propagation of the light through the crystal, whereas the strong absorption of the pure Fe crystals only results in the photoexcitation of the complexes close to the surface and not in the bulk.

DISCUSSION

T(LIESST). In the quest for high T(LIESST) values, chemists have searched for parameters allowing to rationalize and predict the T(LIESST) value, in order to reach the highest T(LIESST) possible. Létard et al. have proposed a relationship between T(LIESST) and $T_{1/2}$ for Fe(II) complexes.[21] They proposed that these two experimental parameters are related by a linear relationship, $T(LIESST) = T_0 - 0.3T_{1/2}$. T_0 has been proposed to be equal to 100, 120, 150, 180, and 200 K for monodentate, bidentate, tridentate, and macrocyclic ligands and Prussian Blue

dx.doi.org/10.1021/ja402674x | J. Am. Chem. Soc. 2013, 135, 8655−8667

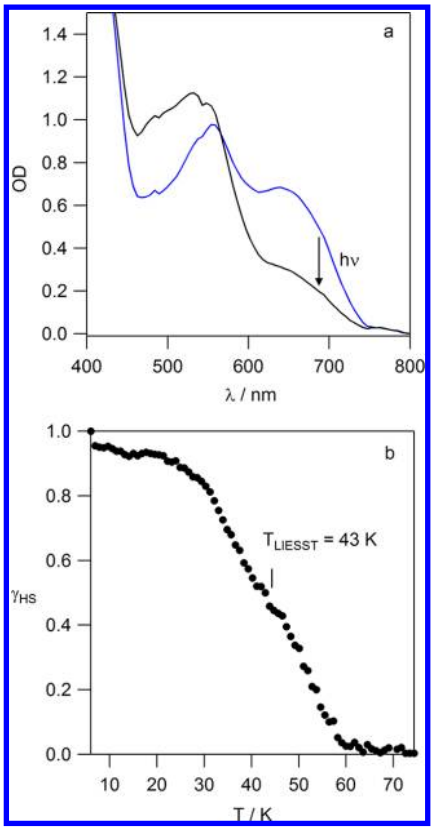

Figure 9. (a) Absorption spectra before and after irradiation at 4 K with light from 690 nm laser of **3·CH_2Cl_2**. (b) Evolution of the photoexcited HS fraction during a heating cycle at 0.3 K/min after irradiation at 4 K on a crystal of **3·CH_2Cl_2**.

analogs, respectively. Sato et al. have looked for an analogous relationship for the Fe^{III} complexes presenting a LIESST effect. Thus, they reported a linear relationship T(LIESST) = T_0 − 0.4$T_{1/2}$, with T_0 = 185 K for the six compounds derived from the $[Fe(pap)]^+$ complex.[8c] In a second article, two more examples of Fe^{III} complexes presenting a LIESST effect containing the complex $[Fe(qsal)_2]^+$ were added.[9] These two compounds were shown to have substantially lower T(LIESST) values than expected from the above relation.

The T(LIESST)/$T_{1/2}$ values for the SCO compounds based on $[Fe^{III}(sal_2\text{-trien})]^+$ inserted into bimetallic oxalate networks as well as the other compounds reported by Sato et al.[8,9] are given in Table 4 and Figure 10.

All the $[Fe(pap)_2]^+$ complexes (points 1−6) lie quite close to the line with T_0 = 150 K, the one obtained for tridentate ligands in Fe^{II} complexes using the relation of Létard et al.[20] Since the pap^- ligand is tridentate in nature, it can be supposed that the Fe^{III} complexes exhibiting a LIESST effect follow the same law as Fe^{II} complexes. The two $[Fe(qsal)_2]^+$ compounds (points 7 and 8) lie sensibly below this line, although the $qsal^-$ ligand is also tridentate. Sato et al. indicated that this could be due to the incomplete LIESST effect of this complex.[9] The four $[Fe^{III}(sal_2\text{-trien})][Mn^{II}Cr^{III}(ox)_3]\cdot S$ (S = CH_2Cl_2, $CHCl_3$, CH_2Br_2, $CHBr_3$) compounds (points 9−12) lie notably lower than the previous Fe^{III} compounds. This behavior is significantly different to that of the pap^- ligand. Indeed, the $sal_2\text{-trien}^{2-}$ ligand is a hexadentate ligand. Thus, a priori, we would have expected the T(LIESST)/$T_{1/2}$ points to be situated on an upper line (T_0 = 180 K for example). A possible explanation may be related to the flexibility of the ligand. Tridentate pap^- and $qsal^-$ ligands are both entirely conjugated in contrast to the $sal_2\text{-trien}^{2-}$ ligand, which possesses three flexible ethylene bridges −CH_2CH_2−. A high flexibility has been recognized as a factor decreasing T(LIESST).[21]

Table 4. $T_{1/2}$ and T(LIESST) for Different Reported Fe(III) Complexes

Nb	$T_{1/2}$/K	T(LIESST)/K	compound
1	174	106	$[Fe(pap)_2]ClO_4\cdot H_2O$
2	189	115	$[Fe(pap)_2]BF_4\cdot H_2O$
3	289	60	$[Fe(pap)_2]PF_6\cdot CH_3OH$
4	293	45	$[Fe(CH_3\text{-pap})_2]ClO_4\cdot H_2O$
5	291	53	$[Fe_{0.5}Al_{0.5}(pap)_2]ClO_4\cdot CH_3OH$
6	350	41	$[Fe_{0.25}Al_{0.75}(pap)_2]ClO_4\cdot CH_3OH$
7	247	40	$[Fe(qsal)_2]NCS$[a]
8	247	50	$[Fe(qsal)_2]NCSe$[a]
9	255	41	**1·CH_2Cl_2**
10	180	58	**1·$CHCl_3$**
11	225	45	**1·CH_2Br_2**
12	142	62	**1·$CHBr_3$**
13	220[b]	45	**2·CH_2Cl_2**
14	225	43	**3·CH_2Cl_2**

[a]These two compounds present only a low light-induced HS fraction. [b]Partial transition only.

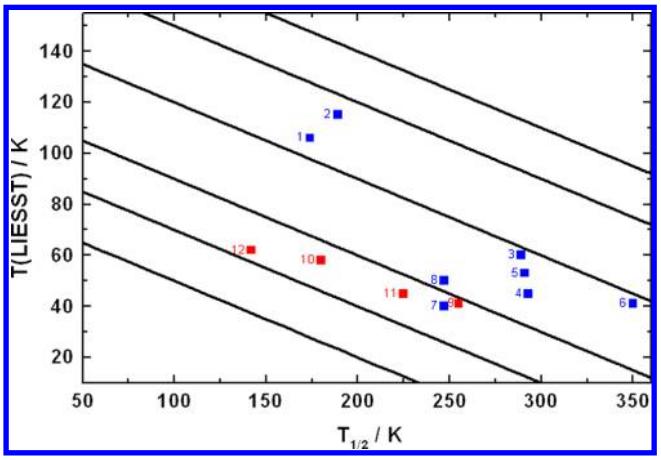

Figure 10. T(LIESST)/$T_{1/2}$ of different Fe^{III} compounds. Blue points are for $[Fe(pap)]^+$ and $[Fe(qsal)_2]^+$, whereas red points are for $[Fe^{III}(sal_2\text{-trien})][Mn^{II}Cr^{III}(ox)_3]\cdot S$ (S = CH_2Cl_2, $CHCl_3$, CH_2Br_2, $CHBr_3$). Parallel lines are for T(LIESST) = T_0 − 0.3$T_{1/2}$, with T_0 = 80, 100, 120, 150, 180, and 200 K.

Sato et al. have related the low T(LIESST) of $[Fe(qsal)_2]$-NCS and $[Fe(qsal)_2]$NCSe to the low photoconversion. Approximately 17% and 8% of LS species were transformed into photoinduced HS species at 5 K for $[Fe(qsal)_2]$NCS and $[Fe(qsal)_2]$NCSe, respectively. It seems however, that in $[Fe^{III}(sal_2\text{-trien})][Mn^{II}Cr^{III}(ox)_3]\cdot S$ compounds, the situation is more complex. For example, **1·$CHCl_3$** presents a T(LIESST) of 58 K with a photoconversion of about 40%, whereas **1·$CHBr_3$** presents a slightly higher T(LIESST) of 62 K with a photoconversion of about 26%. In the dilute system **3·CH_2Cl_2**, the photoconversion is 100% and T(LIESST) is 43 K.

Origin of the LIESST Effect in Fe^{III} Complexes. The lifetime of the HS photoexcited state has been rationalized on the basis of a nonadiabatic mutiphonon relaxation model.[22] Within the framework of this theory, the single configurational coordinate (SCC) approach considers the metal−ligand distance as the reaction coordinate, related to only one

dx.doi.org/10.1021/ja402674x | J. Am. Chem. Soc. 2013, 135, 8655−8667

vibrational mode, the completely symmetrical one. According to SCC theory, the low-temperature (tunneling regime) lifetime of the HS state for Fe^{III} spin-crossover compounds is expected to be of the order of milliseconds, whereas it can go from seconds to months for Fe^{II} spin-crossover compounds. With this short lifetime, it should be impossible to observe the decay of the photoinduced state for Fe^{III} by using standard SQUID techniques. However, as mentioned above, the LIESST effect has been observed by Sato et al. in several Fe^{III} complexes.[8−10] These authors attributed their observations to the strong distortion of the Fe^{III} site from octahedral geometry, enhanced by the presence of strong intermolecular interactions, such as $\pi-\pi$ stacking. Thus, when passing from the ideal octahedral $[Fe^{II}N_6]$ site to a distorted $[Fe^{III}N_4O_2]$ geometry, in addition to the completely symmetrical vibrational mode, other vibrational modes, such as bending modes, should also be taken into account.[9,23] This results in a displacement between the potential walls of the HS and LS states, which is larger than that expected considering only the changes in metal−ligand distances and could explain the long lifetime of the photogenerated HS state.

To evaluate the structural changes of $[Fe(sal_2\text{-trien})]^+$ in **1·CH$_2$Cl$_2$**, **1·CH$_2$Br$_2$**, **1·CHCl$_3$**, and **1·CHBr$_3$**, we have focused our attention on the differences between the 100 and 300 K structures as they are close to the LS and HS structures. A limitation of this comparison is that we assume the photoinduced and high-temperature HS states to present similar structures. X-ray structure determination of crystals of **1·CH$_2$Cl$_2$** after light irradiation at 10 K is in progress to verify this.

As the shortening in the Fe−N and Fe−O bond lengths between the HS and LS structures in these compounds are similar to those of other Fe^{III} complexes, other structural factors, such as the distortion of the octahedral geometry, may be at the origin of the LIESST effect in these compounds. To evaluate and compare this distortion with that of other Fe^{III} complexes, we have used the program SHAPE that can be obtained from its authors upon request.[24] This program calculates continuous shape measures of a set of points (e.g., atomic positions) relative to the vertices of ideal polyhedra and has already been used to find structure−property correlations in SCO complexes.[25] It also calculates the path deviation function for the minimal distortion interconversion path between the two ideal polyhedra (octahedron and a trigonal prism in our case). In the present case, SHAPE calculations show that at all temperatures, the coordination geometry around Fe falls along the minimal distortion path between a perfect octahedron and a perfect trigonal prism with a deviation of <10%. We have then calculated the generalized coordinate between the two ideal polyhedra that gives the trigonal prismacity of a given coordination sphere with respect to a pure octahedron. Thus, complexes with a perfect octahedral geometry or a perfect trigonal prismatic one would have generalized coordinate values of 0% and 100%, respectively. Figure 11 shows that the changes of the generalized coordinate of the Fe^{III} complexes of **1·CH$_2$Cl$_2$** with the temperature follow the same trend as the increase of HS fraction extracted from magnetic and Mössbauer measurements.[5] The distortion of the octahedral geometry of these complexes from the LS to the HS state follows then a Bailar twist with a higher distortion for the HS state. The trigonal prismacity of the Fe^{III} complexes of **1·CHCl$_3$**, **1·CHBr$_3$**, and **1·CH$_2$Br$_2$** in the LS and HS states are similar to those of **1·CH$_2$Cl$_2$** at the same temperatures with small

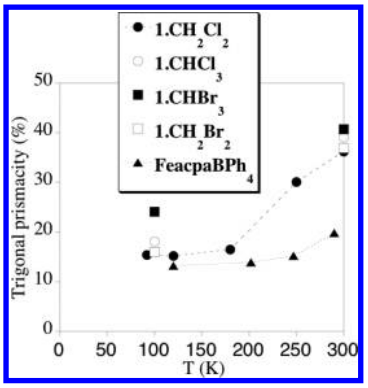

Figure 11. Trigonal prismacity of **1·CHBr$_3$**, **1·CHCl$_3$**, **1·CH$_2$Br$_2$**, **1·CH$_2$Cl$_2$**, and $[Fe(acpa)]BPh_4$ at different temperatures calculated with the SHAPE program.

differences that can be related to small differences in the LS/HS ratio (see Figure 11). Therefore, the HS Fe^{III} complexes in **1·CH$_2$Cl$_2$**, **1·CHCl$_3$**, **1·CHBr$_3$**, and **1·CH$_2$Br$_2$** present a Bailar distortion with respect to the LS complexes.

To see whether the LIESST effect could be related to this distortion, the trigonal distortion of other $[Fe(sal_2\text{-trien})]^+$ salts in which LIESST is not detected, such as the reference compound, $[Fe(sal_2\text{-trien})]ClO_4$ and the compound $[Fe^{III}(sal_2\text{-trien})][Mn^{II}Cr^{III}(ox)_3]\cdot CH_3OH$, was calculated.[5,7,26] The results show that they present a similar trigonal distortion as those of $[Fe(sal_2\text{-trien})]^+$ salts presenting a LIESST effect.[27] Then, the same method was used to evaluate the distortion of other Fe^{III} complexes not presenting a LIESST effect such as $[Fe(acpa)_2]^+$. This complex presents a Bailar twist in $[Fe(acpa)_2]BPh_4$ that follows the same trend as the magnetic measurements (see Figure 11), but the relative changes are much smaller than those found for the $[Fe^{III}(sal_2\text{-trien})]^+$ salts. Finally, the distortion of the octahedral geometry of $[Fe^{III}(pap)_2]^+$, the Fe^{III} complex exhibiting the clearest LIESST effect, has been evaluated. In this case the coordination geometry is far from the pure octahedral one even for the LS state. In contrast to $[Fe(sal_2\text{-trien})]^+$ complexes, the changes of the coordination sphere from LS to HS do not follow a Bailar distortion. This may be related to the tridentate character of the pap ligands that favors a different type of distortion path (D_{2d}) rather than the trigonal twist.[25a]

We conclude that the Fe^{III} complexes exhibiting a LIESST effect present a large distortion of the octahedral geometry in their HS state. However, in $[Fe^{III}(sal_2\text{-trien})]^+$ salts, other factors may contribute to this rare property as several salts of this cation with a similar distortion of the octahedral geometry do not present a LIESST effect, such as the ClO_4^- and 3D $[Mn^{II}Cr^{III}(ox)_3]^-$ salts. In the case of $[Fe^{III}(pap)_2]^+$ salts, which present a different distortion of the octahedral geometry between the LS and HS states, it has been proposed that cooperative interactions due to strong $\pi-\pi$ stacking intermolecular interactions may be at the origin of the LIESST effect. This factor cannot be used to explain the LIESST effect of $[Fe^{III}(sal_2\text{-trien})]^+$ compounds as they do not present abrupt spin-crossover transitions characteristic of cooperative systems. Furthermore, spectroscopic measurements on single crystals of the doped compound **3·CH$_2$Cl$_2$**, which is isostructural to **1·CH$_2$Cl$_2$**, confirm that the LIESST effect in this type of compound is not related to cooperativity. An important structural difference between the compounds reported in this paper and the other Fe^{III} compounds exhibiting a LIESST effect

dx.doi.org/10.1021/ja402674x | J. Am. Chem. Soc. 2013, 135, 8655−8667

is the presence of the bimetallic, anionic extended oxalate network, instead of discrete small counterions. This rigid network could play an important role in the stabilization of the metastable HS state. In favor of this hypothesis is the numerous short contacts between the $[Fe(sal_2\text{-trien})]^+$ cations and the oxalate ligands, which are different in the low- and high-temperature structures. These interactions may stabilize the photogenerated LIESST complex and prevent fast relaxation to the LS ground state. In other words, the increase of volume of the $[Fe^{III}(sal_2\text{-trien})]^+$ complexes after the photoinduced spin-crossover may result in new interactions with the bimetallic oxalate layers, which prevent fast relaxation to the LS ground state. A structure determination of the metastable LIESST state is in progress to confirm this hypothesis, but this is not a trivial task.

Possible explanations for the absence of LIESST in other $[Fe(sal_2\text{-trien})]^+$ complexes inserted in 2D or 3D extended oxalate-based networks are:[7,11c] (a) a too high $T_{1/2}$ leading to a too fast HS−LS relaxation to be detected on the time scale of SQUID measurements; (b) the small amount of Fe^{III} that can undergo SCO; and (c) a different organization of the $[Fe(sal_2\text{-trien})]^+$ complexes in which only weak contacts with the oxalate network are established. Synthesis of more Fe^{III} complexes showing LIESST together with further characterization is needed to understand this unusual property.

CONCLUSION

We have demonstrated that the substitution of CH_2Cl_2 for other halogenated solvents in the synthesis of the 2D oxalate-based ferromagnet of formula $[Fe^{III}(sal_2\text{-trien})][Mn^{II}Cr^{III}(ox)_3]\cdot CH_2Cl_2$ permits the preparation of a family of compounds with an analogous structure that maintain the interesting physical properties of this compound, i.e., a coexistence of magnetic ordering and the LIESST effect. The subtle structural changes provide a model system for studying in detail the LIESST effect in Fe^{III} complexes. In fact, the change of solvent modifies the chemical pressure exerted on the inserted cation leading to different temperatures of the thermal and photoinduced SCO for each compound. Thus, the bulkiest $CHBr_3$ solvent increases the interlayer separation between layers in the structure of **1·CHBr$_3$** and favors the HS state, while the opposite is observed for the solvent of smallest volume, that is, CH_2Cl_2. As a consequence, **1·CHBr$_3$** and **1·CH$_2$Cl$_2$** present, respectively, the lowest and highest $T_{1/2}$ and the highest and lowest T(LIESST) of this family of compounds. Therefore, substitution of CH_2Cl_2 in **1·CH$_2$Cl$_2$** by the bulkier $CHBr_3$, CH_2Br_2, and $CHCl_3$ solvent molecules has proven to be a successful strategy to obtain Fe^{III} complexes exhibiting a LIESST effect at higher temperatures.

The versatility of this system has also allowed us to show that the replacement of Fe^{III} complexes by the diamagnetic Ga^{III} is a successful strategy to perform a spectroscopic characterization on single crystals. Thus, we have demonstrated that $[Ga_{1-x}Fe_x(sal_2trien)][Mn^{II}Cr^{III}(ox)_3]\cdot CH_2Cl_2$, $x = 0.01$ (**3·CH$_2$Cl$_2$**), also presents a complete thermal SCO and a quantitative LIESST effect. These measurements on diluted samples confirm that, in contrast to the results obtained by Sato et al.,[8,9] cooperativity is not a necessary condition to observe the LIESST effect in Fe^{III} complexes, as cooperativity is excluded in these doped systems due to the long distance between the Fe^{III} centers.

Structural analysis of these compounds and other Fe^{III} complexes indicates that several factors may explain the LIESST effect in Fe^{III} complexes. In the case of $[Fe^{III}(pap)_2]^+$ complexes, the presence of a rigid tridentate ligand that induces a distorted octahedral geometry together with strong $\pi-\pi$ interactions between the Fe^{III} complexes could be at the origin of this effect, while in the $[Fe^{III}(sal_2\text{-trien})]^+$ complexes reported here, which contain a more flexible ligand, it could be related to the interactions with a bimetallic oxalate extended network. Further experiments are needed to confirm this point.

In conclusion, this work confirms that the confinement of SCO cations into extended networks based on oxalate complexes is a suitable strategy to induce LIESST effect on Fe^{III} molecules. This opens the way to the use of this hybrid approach for the preparation of new multifunctional materials coupling the switching properties of the SCO molecule with a second property coming from the extended network (magnetism, conductivity, etc.).

ASSOCIATED CONTENT

Supporting Information

Powder X-ray diffraction patterns of **1·CH$_2$Br$_2$**, **1·CHCl$_3$**, and **1·CHBr$_3$**; magnetization curves of **1·CH$_2$Br$_2$**, **1·CHCl$_3$**, and **1·CHBr$_3$**; the temperature dependence of $\chi_M T$ for **2·CH$_2$Cl$_2$**; relaxation kinetics and simulation of the $\chi_M T$ product vs time at different temperatures of **1·CH$_2$Br$_2$**, **1·CHCl$_3$**, and **1·CHBr$_3$**; temperature dependence of the estimated relative areas of HS Fe^{III} from the Mössbauer spectra for compounds **1·CH$_2$Br$_2$**, **1·CHCl$_3$**, and **1·CHBr$_3$** and tables with the intermolecular contacts and the parameters from the relaxation kinetics curves of **1·CH$_2$Br$_2$**, **1·CHCl$_3$**, and **1·CHBr$_3$**. This material is available free of charge via the Internet at http://pubs.acs.org.

AUTHOR INFORMATION

Corresponding Author

miguel.clemente@uv.es; eugenio.coronado@uv.es

Notes

The authors declare no competing financial interest.

ACKNOWLEDGMENTS

Financial support from the European Union (HINTS and SPINMOL ERC Advanced Grant), the Spanish Ministerio de Economía y Competitividad (Projects Consolider-Ingenio in Molecular Nanoscience CSD2007-00010, MAT2011-22785, and CTQ-2011-26507), and the Generalitat Valenciana (Prometeo and ISIC programs) are gratefully acknowledged. The authors also thank J. M. Martínez-Agudo and Dr. Gloria Agustí-López, University of Valencia, for magnetic characterization of the samples, Prof. S. Hayami and Prof. O. Sato by kindly providing the structural data of $[Fe^{III}(pap)_2]PF_6.CH_3OH$ compound and Prof. S. Alvarez by kindly providing the SHAPE program and for helpful discussions. A.T. acknowledges a Marie-Curie Fellowship of the European Union. C. Besnard is acknowledged for the structure determination of the compound **3·CH$_2$Cl$_2$**.

REFERENCES

(1) (a) Coronado, E.; Day, P. *Chem. Rev.* **2004**, *104*, 5419. (b) Coronado, E.; Martí-Gastaldo, C.; Navarro-Moratalla, E.; Ribera, A.; Blundell, S. J.; Baker, P. J. *Nat. Chem.* **2010**, *2*, 1031. (c) Coronado, E.; Martí-Gastaldo, C.; Navarro-Moratalla, E.; Burzuri, E.; Camon, E.; Luis, F. *Adv. Mater.* **2011**, *23*, 5021.

(2) Coronado, E.; Mínguez Espallargas, G. *Chem. Soc. Rev.* **2013**, *42*, 1525.
(3) (a) Sato, O.; Iyoda, T.; Fujishima, A.; Hashimoto, K. *Science* **1996**, *272*, 704. (b) Coronado, E.; Giménez-López, M. C.; Levchenko, G.; Romero, F. M.; García-Baonza, V.; Milner, A.; Paz-Pasternak, M. *J. Am. Chem. Soc.* **2005**, *127*, 4580. (c) Coronado, E.; Giménez-López, M. C.; Korzeniak, T.; Levchenko, G.; Romero, F. M.; Segura, A.; García-Baonza, V.; Cezar, J. C.; De Groot, F. M. F.; Milner, A.; Paz-Pasternak, M. *J. Am. Chem. Soc.* **2008**, *130*, 15519. (d) Ohkoshi, S.−I.; Imoto, K.; Takano, S.; Tokoro, H. *Nat. Chem.* **2011**, *3*, 564.
(4) (a) Bénard, S.; Yu, P.; Audière, J. P.; Rivière, E.; Clèment, R.; Ghilhem, J.; Tchertanov, L.; Nakatami, K. *J. Am. Chem. Soc.* **2000**, *122*, 9444. (b) Coronado, E.; Galán-Mascarós, J. R.; Gómez-García, C. J.; Laukhin, V. *Nature* **2000**, *408*, 447. (c) Train, C.; Gheorghe, R.; Krstic, V.; Chamoreau, L. M.; Ovanesyan, N. S.; Rikken, G. L. J. A.; Gruselle, M.; Verdaguer, M. *Nat. Mater.* **2008**, *7*, 729. (d) Okawa, H.; Shigematsu, A.; Sadakiyo, M.; Miyagawa, T.; Yoneda, K.; Ohba, M.; Kitagawa, H. *J. Am. Chem. Soc.* **2009**, *131*, 13516. (e) Train, C.; Nuida, T.; Gheorghe, R.; Gruselle, M.; Ohkoshi, S. *J. Am. Chem. Soc.* **2009**, *131*, 16838. (f) Clemente-León, M.; Coronado, E.; Martí-Gastaldo, C.; Romero, F. M. *Chem. Soc. Rev.* **2011**, *40*, 473. (g) Pardo, E.; Train, C.; Liu, H.; Chamoreau, L.-M.; Dkhil, B.; Boubekeur, K.; Lloret, F.; Nakatani, K.; Tokoro, H.; Ohkoshi, S.-I.; Verdaguer, M. *Angew. Chem., Int. Ed.* **2012**, *51*, 8356. (h) Sadayiko, M.; Okawa, H.; Shigematsu, A.; Ohba, M.; Yamada, T.; Kitagawa, H. *J. Am. Chem. Soc.* **2012**, *134*, 5472. (i) Okawa, H.; Sadakiyo, M.; Yamada, T.; Maesato, M.; Ohba, M.; Kitagawa, H. *J. Am. Chem. Soc.* **2013**, *135*, 2256.
(5) Clemente-León, M.; Coronado, E.; López-Jordà, M.; Mínguez Espallargas, G.; Soriano-Portillo, A.; Waerenborgh, J. C. *Chem.—Eur. J.* **2010**, *16*, 2207.
(6) (a) Decurtins, S.; Gütlich, P.; Köhler, C. P.; Spiering, H.; Hauser, A. *Chem. Phys. Lett.* **1984**, *105*, 1. (b) Hauser, A. *Top. Curr. Chem.* **2004**, *234*, 155.
(7) Clemente-León, M.; Coronado, E.; López-Jordà, M.; Desplanches, C.; Asthana, S.; Wang, H.; Létard, J.-F. *Chem. Sci.* **2011**, *2*, 1121.
(8) (a) Hayami, S.; Gu, Z. −Z.; Shiro, M.; Einaga, Y.; Fujishima, A.; Sato, O. *J. Am. Chem. Soc.* **2000**, *122*, 7126. (b) Juhász, G.; Hayami, S.; Sato, O.; Maeda, Y. *Chem. Phys. Lett.* **2002**, *364*, 164. (c) Hayami, S.; Kawahara, T.; Maeda, Y.; Inoue, K.; Sato, O. *J. Radioanal. Nucl. Chem.* **2005**, *266*, 521.
(9) Hayami, S.; Hiki, K.; Kawahara, T.; Maeda, Y.; Urakami, D.; Inoue, K.; Ohama, M.; Kawata, S.; Sato, O. *Chem.—Eur. J.* **2009**, *15*, 3497.
(10) Shimizu, T.; Komatsu, Y.; Kamihata, H.; Lee, Y. H.; Fuyuhiro, A.; Iijima, S.; Hayami, S. *J. Inclusion Phenom. Mol. Recognit. Chem.* **2011**, *71*, 363.
(11) (a) Clemente-León, M.; Coronado, E.; López-Jordà, M. *Dalton Trans.* **2010**, *39*, 4903. (b) Clemente-León, M.; Coronado, E.; López-Jordà, M.; Waerenborgh, J. C. *Inorg. Chem.* **2011**, *50*, 9122. (c) Clemente-León, M.; Coronado, E.; López-Jordà, M. *Eur. J. Inorg. Chem.* **2013**, 753.
(12) Tweedle, M. F.; Wilson, L. J. *J. Am. Chem. Soc.* **1976**, *98*, 4824.
(13) Baylar, J. C.; Jones, E. M. *Inorganic Synthesis*; Booth, H. S.; Ed.; McGraw-Hill: New York, 1939; Vol. *1*, p 35.
(14) Altomare, A.; Burla, M. C.; Camalli, M.; Cascarano, G. L.; Giacovazzo, C.; Guagliardi, A.; Moliterni, A. G. G.; Polidori, G.; Spagna, R. *J. Appl. Crystallogr.* **1999**, *32*, 115.
(15) Sheldrick, G. M. *SHELXL-97*; University of Göttingen: Göttingen, Germany, 1997.
(16) Farrugia, L. J. *J. Appl. Crystallogr.* **1997**, *32*, 837.
(17) Rodrigues, J. V.; Santos, I. C.; Gama, V.; Henriques, R. T.; Waerenborgh, J. C.; Duarte, M. T.; Almeida, M. *J. Chem. Soc., Dalton Trans.* **1994**, 2655.
(18) Unit cell of compound $[In^{III}(sal_2\text{-trien})][Mn^{II}Cr^{III}(ox)_3]$ obtained in CH_2Cl_2 measured with single crystal X-ray diffraction (a = 15.841(12) Å, b = 20.639(16) Å and c = 21.285(18) Å, β = 90°, V = 6947(10)Å^3) is similar to that of other 3D compounds obtained in CH_3CN or CH_3NO_2, such as compound **4** from ref 5.
(19) Unit cell of compound $[Ga^{III}(sal_2\text{-trien})][Mn^{II}Cr^{III}(ox)_3]\cdot CH_2Cl_2$ measured with single crystal X-ray diffraction (a = 11.851(8) Å, b = 31.972(18) Å and c = 9.486(7)Å, β = 111.62(6)°, V = 3342(4)Å^3) is similar to that of the 2D compound obtained in CH_2Cl_2 with $[Fe^{III}(sal_2\text{-trien})]$ (**1**·CH_2Cl_2).
(20) Mishra, V.; Mukherjee, R.; Linares, J.; Baldé, C.; Desplanches, C.; Létard, J.-F.; Collet, E.; Toupet, L.; Castro, M.; Varret, F. *Inorg. Chem.* **2008**, *47*, 7577.
(21) (a) Létard, J.-F.; Guionneau, P.; Nguyen, O.; Sanchez Costa, J.; Marcen, S.; Chastanet, G.; Marchivie, M.; Goux-Capes, L. *Chem.—Eur. J.* **2005**, *11*, 4582. (b) Létard, J.-F. *J. Mater. Chem.* **2006**, *16*, 2550.
(22) Hauser, A. *J. Chem. Phys.* **1991**, *94*, 2741.
(23) Schenker, S.; Hauser, A.; Dyson, R. M. *Inorg. Chem.* **1996**, *35*, 4676.
(24) Llunell, M.; Casanova, D.; Cirera, J.; Bofill, J. M.; Alemany, P.; Alvarez, S.; Pinski, M.; Avnir. D. *SHAPE (2.0)*; Barcelona, 2010.
(25) (a) Alvarez, S. *J. Am. Chem. Soc.* **2003**, *125*, 6795. (b) Matouzenko, G. S.; Borshch, S. A.; Jeanneau, E.; Bushuev, M. B. *Chem.—Eur. J.* **2009**, *15*, 1252.
(26) Pritchard, R.; Barrett, S. A.; Kilner, C. A.; Halcrow, M. A. *Dalton Trans.* **2008**, 3159.
(27) Trigonal prismacity of the two crystallographically independent iron atoms of $[Fe^{III}(sal_2\text{-trien})][Mn^{II}Cr^{III}(ox)_3]\cdot CH_3OH$ is 29.1 and 34.9% at 120 K, temperature at which 70% of Fe^{III} is in the HS state. Trigonal prismacity of the four crystallographically independent iron atoms of $[Fe^{III}(sal_2\text{-trien})]ClO_4$ is 37.4 and 41.8% for the HS Fe^{III} and 14.1 and 19.2% for the LS Fe^{III} at 105 K. At this temperature half of the Fe^{III} is in the HS state (see ref 26).